# Europe's Lost Frontiers

General Editor
Vincent Gaffney

Volume 1

## Context and Methodology

edited by
Vincent Gaffney and Simon Fitch

ARCHAEOPRESS

# Europe’s Lost Frontiers

## Volume 1

## Context and Methodology

edited by

Vincent Gaffney and Simon Fitch

general editor
Vincent Gaffney

Archaeopress Archaeology

Archaeopress Publishing Ltd
Summertown Pavilion
18-24 Middle Way
Summertown
Oxford OX2 7LG

www.archaeopress.com

ISBN 978-1-80327-268-9
ISBN 978-1-80327-269-6 (e-Pdf)



Cover: Eleanor Ramsey

Landing by Ava Grauls (Duncan of Jordanstone College of Art & Design).
Oil and watercolour on Japanese shōji (障子) paper. 413 x 244cm

Landing is about location, ownership, shifting land and shifting borders. The painting was conceived after talking to academics about the space between Britain and Europe, and asking the question: 'How do you paint a forgotten landscape?' Landing was made to travel and interact with different environments and can be folded up and packed away into four boxes.
Ava Grauls 11/08/2021

Dedicated to our Families
For putting up with Doggerland for longer than any families since the Mesolithic

November 2021

# Europe’s Lost Frontiers

**Europe’s Lost Frontiers** was funded through a European Research Council Advanced Grant (project number 670518). The European Research Council’s mission is to encourage the highest quality research in Europe through competitive funding and to support investigator-driven frontier research across all fields, on the basis of scientific excellence. The European Research Council complements other funding activities in Europe such as those of the national research funding agencies, and is a flagship component of Horizon Europe, the European Union's Research Framework Programme.

European Research Council

Established by the European Commission

# Contents

## Supplementary Data

# List of Figures

# List of Tables

# The Lost Frontiers Team

**University of Bradford**
Dr Andrew Fraser
Dr Ben Stern
Dr Catherine Batt
Dr James Walker
Dr Philip Murgatroyd
Dr Rachel Harding
Dr Richard Telford
Dr Simon Fitch
Dr Tabitha Kabora
Micheál Butler
Mohammed Bensharada
Professor Vincent Gaffney
Sam Harris
Dr Helen McCrearey
Elizabeth Topping
Anne Harvey
Tim Squire-Watt

**University of Aberystwyth**
Professor Sarah Davies

**University of Bath**
Dr Matt Law

**University of Birmingham**
Dr David Smith
Eamonn Baldwin

**Chemostrat**
Dr Alexander Finlay

**University College Cork**
Dr Ben Gearey
Dr Kevin Kearney

**Flanders Marine Institute**
Dr Tine Missiaen
Dr Ruth Plets

**National University of Ireland, Galway**
Eoghan Daly

**University of Glasgow**
Dr Derek Hamilton

**INFOMAR**
Kevin Sheehan

**Natural History Museum**
Dr John Whittaker

**University of Nottingham, Ningbo**
Professor Eugene Ch'ng

**PalaeoEnvironmental Research and Consultancy Services Ltd**
Dr Tom Hill

**Sligo Institute of Technology**
Dr James Bonsall
Eithne Davis

**University of Wales, Trinity St Davids**
Dr Martin Bates
Erin Kavanagh

**University of St Andrews**
Professor Richard Bates
Dr Tim Kinnaird
Rebecca Bateman
Aayush Srivastava

**University of Tartu**
Dr Merle Muru
Dr Alar Rosentau

**University of Warwick**
Dr Rebecca Cribdon
Dr Roselyn Ware
Professor Robin Allaby
Dr Rosie Everett

**Wolverhampton and Walsall Historic Environment Record**
Eleanor Ramsey

Dr Martin Tingle
Dr Wendy Carruthers

# Authors' details

Robin Allaby, School of Life Sciences, Gibbet Hill Campus, University of Warwick, Coventry CV4 7AL, United Kingdom

Rebecca Bateman, School of Earth and Environmental Sciences, University of St Andrews, Bute Building, Queen's Terrace, St Andrews KY16 9TS. United Kingdom

Martin Bates, Faculty of Humanities and Performing Arts, University of Wales Trinity Saint David, Lampeter, Ceredigion SA48 7ED, United Kingdom

Richard Bates, School of Earth and Environmental Sciences, University of St Andrews, Bute Building, Queen's Terrace, St Andrews KY16 9TS, United Kingdom

Catherine M. Batt, School of Archaeological and Forensic Sciences, University of Bradford, Richmond Road, Bradford BD7 1DP, United Kingdom

Mohammed Bensharada, School of Archaeological and Forensic Sciences, University of Bradford, Richmond Road, Bradford BD7 1DP, United Kingdom

Micheál Butler, School of Archaeological and Forensic Sciences, University of Bradford, Richmond Road, Bradford BD7 1DP, United Kingdom

Eugene Ch'ng, NVIDIA Technology Centre, University of Nottingham Ningbo China, 199 Taikang East Road, Ningbo 315100, China

Rebecca Cribdon, School of Life Sciences, Gibbet Hill Campus, University of Warwick. Coventry CV4 7AL, United Kingdom

Sarah Davies, School of Geography and Earth Sciences, Llandinam Building, Penglais Campus, Aberystwyth University, Aberystwyth SY23 3DB, United Kingdom.

Rosie Everett, School of Life Sciences, Gibbet Hill Campus, University of Warwick. Coventry CV4 7AL, United Kingdom

Alexander Finlay, Chemostrat Ltd., 1 Ravenscroft Court, Buttington Cross Enterprise Park, Welshpool, Powys SY21 8SL, United Kingdom

Simon Fitch, School of Archaeological and Forensic Sciences, University of Bradford, Richmond Road, Bradford BD7 1DP, United Kingdom

Andrew Fraser, School of Archaeological and Forensic Sciences, University of Bradford, Richmond Road, Bradford BD7 1DP, United Kingdom

Vincent Gaffney, School of Archaeological and Forensic Sciences, University of Bradford, Richmond Road, Bradford BD7 1DP, United Kingdom

Ben Gearey, Department of Archaeology, Connolly Building, Dyke Parade, University College, Cork, Cork City T12 CY82, Ireland

Derek Hamilton, Scottish Universities Environmental Research Centre, Rankine Avenue, Scottish Enterprise Technology Park, East Kilbride G75 0QF, United Kingdom

Rachel Harding, School of Archaeological and Forensic Sciences, University of Bradford, Richmond Road, Bradford BD7 1DP, United Kingdom

Samuel E. Harris , School of Archaeological and Forensic Sciences, University of Bradford, Richmond Road, Bradford BD7 1DP, United Kingdom

Tom Hill, PalaeoEnvironmental Research and Consultancy Service, 67 Eastfield Road, Princes Risborough, Buckinghamshire HP27 0HZ / Department of Earth Sciences, The Natural History Museum, Cromwell Road, London SW7 5BD, United Kingdom.

Tabitha Kabora, Leverhulme Centre for Anthropocene Biodiversity, University of York, York YO10 5DD, United Kingdom

Erin Kavanagh, Arts Building, University of Birmingham, Edgbaston, Birmingham B15 2TT, United Kingdom

Tim Kinnaird, School of Earth and Environmental Sciences, University of St Andrews, Bute Building, Queen's Terrace, St Andrews KY16 9TS UK

Philip Murgatroyd, School of Archaeological and Forensic Sciences, University of Bradford, Richmond Road, Bradford BD7 1DP, United Kingdom

Merle Muru, Department of Geography, University of Tartu, 46 Vanemuise Str, 51003 Tartu, Estonia

Eleanor Ramsey, Wolverhampton and Walsall Historic Environment Record, Wolverhampton City Council, Civic Centre, St Peter's Square, Wolverhampton, WV1 1RP, United Kingdom.

David Smith, Classics, ancient History and Archaeology, University of Birmingham, Edgbaston, Birmingham B15 2TT, United Kingdom

Aayush Srivastava, School of Earth and Environmental Sciences, University of St Andrews, Bute Building, Queen's Terrace, St Andrew, KY16 9TS, United Kingdom.

Ben Stern, School of Archaeological and Forensic Sciences, University of Bradford, Richmond Road, Bradford BD7 1DP, United Kingdom

Richard Telford, Centre for Chemical and Biological Analysis, University of Bradford, Richmond Road, Bradford BD7 1DP, United Kingdom

Martin Tingle, 106 Brook Street, Wymeswold LE12 6TU, United Kingdom

Elizabeth Topping, School of Archaeological and Forensic Sciences, University of Bradford, Richmond Road, Bradford BD7 1DP, United Kingdom

James Walker Archaeological Museum, University of Stavanger, 4036 Stavanger, P.O. box 8600, Norway

Roselyn Ware, School of Life Sciences, Gibbet Hill Campus, University of Warwick. Coventry CV4 7AL, United Kingdom

John Whittaker, Department of Earth Sciences, The Natural History Museum, Cromwell Road, London SW7 5BD, United Kingdom.

## Chapter 12

# Constructing sediment chronologies for Doggerland

Tim Kinnaird, Martin Bates, Rebecca Bateman and Aayush Srivastava

### Introduction

Luminescence dating is an important tool for constraining sediment ages and depositional processes in many Quaternary environments. This chapter provides examples of how optically stimulated luminescence, or OSL, has been applied to late Pleistocene to Holocene deposits recovered from core in the southern North Sea, to establish a chronology and define sedimentation histories. These sediment chronologies contribute to the palaeo-environmental reconstructions of Doggerland discussed elsewhere in this volume. Doggerland exhibits a complex palaeo-geography, with sediments deposited in diverse terrestrial, littoral and marine settings (see Bates *et al.* this volume), which presents some challenges to dating these sediments. The chapter begins with a brief consideration of the principles of luminescence dating, followed by a discussion of its application in the context of the North Sea. Then, the 'challenges' associated with OSL are discussed with reference to Doggerland, prior to outlining some potential solutions. Finally, the methods and protocols used in dating Doggerland sediments are discussed, illustrated with the example of establishing a sediment chronology for core ELF001A.

The luminescence dating technique exploits the energy retained in certain minerals, typically quartz and feldspar, which accumulate as a consequence of naturally occurring ionising radiation in both the sample and its environment. These signals are depleted, or reset, when the minerals are exposed to either heat or daylight. 'Zeroing' can be achieved during daylight exposure in phases of erosion or transport. After burial, or deposition, luminescence will grow *in situ* in response to the radioactivity of the surrounding sediment and cosmic rays. This is quantified as the equivalent dose (abbreviated to De), which is determined by calibrating the intensity of the OSL signal against the response to known laboratory-administered radiation doses (in Gray, abbreviated to Gy). To calculate an age, it is also necessary to measure the rate of radioactivity delivered to the sample from the surrounding sediment matrix, and this is called the environmental dose rate. A luminescence age is derived using the equation below:

$$\text{Age (ka)} = \text{Burial dose (Gy)}/\text{Total environmental dose rate (Gy ka}^{-1}\text{)}$$

OSL is routinely used to date sediments in terrestrial environments, as recently reviewed by Smedley (2018) and Rittenour (2018). Marine sediments were first dated by thermoluminescence in 1979 (Wintle and Huntley 1979), and using OSL techniques in 2003 (Stokes *et al.* 2003). Wintle and Huntley (1979; 1980) developed TL dating procedures to date marine sediments, extracted from deep cores in the Antarctic and North Pacific oceans. The ages were stratigraphically coherent, but issues including time-dependent dose rate calculations, anomalous fading in feldspars and large uncertainties, discouraged further applications of TL dating to marine sediments. After a long hiatus, Stokes *et al.* (2003) revisited luminescence dating of marine sediments and applied a single aliquot, regenerative dose (SAR) OSL technique to silt-sized quartz from cores extracted from the Arabian Sea. The authors reported ages that had low standard errors and showed agreements with independent chronometric control. They used thin source alpha spectrometry to examine the uranium (U) and thorium (Th) decay series for time-dependent changes in dose rate.

Since 2003, studies have applied various luminescence dating techniques to a range of different types of coastal and marine deposits, involving a variety of depositional processes and environments (e.g. Armitage 2015; Jacobs 2008; Jakobsson *et al.* 2003; Sanderson and Kinnaird 2019; Tappin *et al.* 2011): establishing OSL dating as a suitable method to determine timing of depositional events in nearshore and offshore marine environments. Bateman (2015) provides a comprehensive review of luminescence dating applied in coastal and marine contexts.

In the North Sea region, there are relatively few comparative studies: Alappet *et al.* (2010) constructed chronologies for shallow terrestrial and marine deposits in the southern North Sea, south east of Dogger Bank. They obtained late Weichselian and early Holocene ages for glacio-fluvial and lacustrine sediments 2.0 to 0.5m beneath the terrestrial-to-marine transition that attested to sedimentation in a predominantly periglacial, fluvial environment. The authors noted significant scatter in the equivalent dose distributions of quartz due to heterogeneous bleaching. Further north and west, offshore the Humber Estuary, Tappin *et al.* (2011) applied a combination of OSL and radiocarbon dating to re-interpret the geological evolution of the area over the last 21,000 years, from when the region was glaciated and the Brown Bank Formation was laid down to marine transgression. Madsen *et al.* (2005) showed that it is possible to date young, fine-grained estuarine deposits by OSL: they obtained OSL sediment ages for a length of core through tidal mudflats in Ho Bugt, ranging from 7.0 ± 1.5 (near surface) to 305 ± 16 years (at 68cm depth), concordant with $^{210}$Pb ages back to *c.* 1975. Moreover, an average OSL age of 9 ± 3 years for the surface mixing zone showed that in this setting the OSL signal of the quartz grains was well-zeroed at deposition.

22 of the 78 sedimentary cores recovered from the Outer Dowsing Deep region of the southern North Sea were investigated in the context of OSL dating and four are referenced within this chapter (Figure 12.1). The objectives of this chapter are, therefore, threefold:

1. to evaluate the potential of OSL for establishing a chronology and sedimentation history of late Pleistocene to Holocene deposits at Dogger Bank
2. to discuss the challenges associated with OSL, with reference to the submerged Doggerland palaeo-environments: partial bleaching, mineralogical variations with varied luminescence response, stable dose rate conditions and disequilibrium in the uranium decay series
3. to review these challenges and design a methodology to date the submerged Doggerland marine, nearshore and terrestrial deposits

This will be the reference to all OSL depositional ages reported in this, and subsequent volumes, in the *Europe's Lost Frontiers* (ELF) monograph series.

## 'Challenges' to dating the sediments of Doggerland

### *Challenge 1: Partial bleaching of sediments*

It is a clear requirement of the technique that the sedimentary grains used as the luminescence dosimeter are exposed to adequate light at deposition to bleach, or zero, the luminescence signals. Where the mineral grains are not exposed to sufficient daylight, we observe a phenomenon known as partial bleaching, which can contribute to significant scatter in determined De values and hence determined ages (Duller 2008; Olley *et al.* 1998). Poor 'zeroing' at deposition leading to large overestimations in age.

The resetting of the luminescence signals during transportation and deposition is a function of environmental conditions and luminescence behaviour (Figure 12.2).

In the littoral zone, the optimum depositional environment is commonly considered to be coastal dunes, because aeolian transport (particularly, saltation) provides a very high probability of daylight exposure prior to burial. Whereas, in intertidal, marsh and lagoonal settings, exposure to daylight prior to burial is less certain, with diminished light penetration

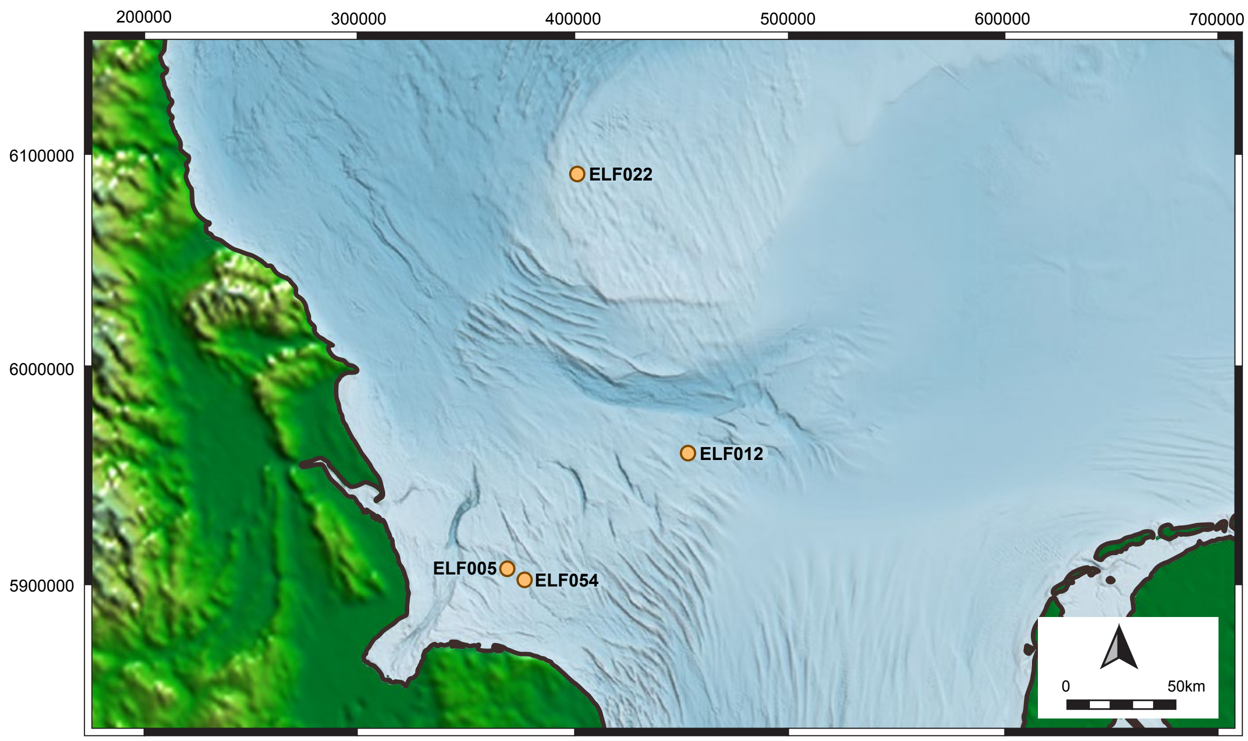


Figure 12.1 Locations of cores mentioned in text.

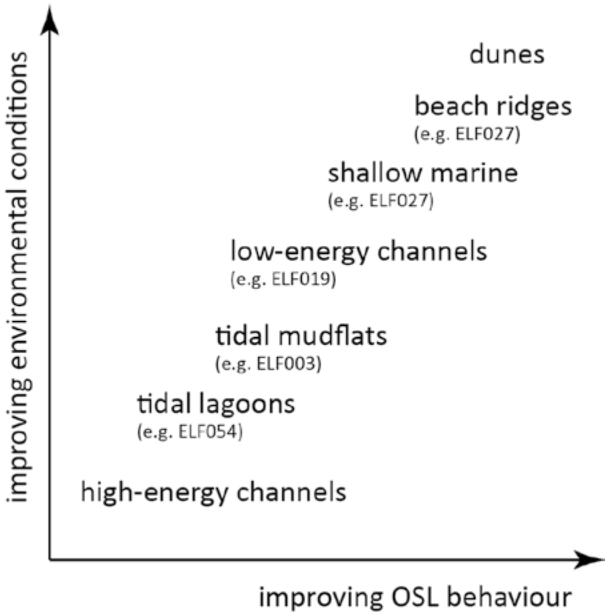


Figure 12.2 For successful OSL dating, both environmental and mineral characteristics are important: zeroing during transport and deposition is a function of environmental conditions and luminescence behaviour.

through the water column, and mixing of suspended sediment with sediments deposited from singular or episodic events (Bateman 2015).

***Challenge 2: Post-depositional sediment mixing***

Post-depositional mixing can be due to bioturbation or geomorphic processes (e.g. sediment slumping). Either phenomena could contribute to further scatter in determined De values and determined ages. Bioturbated sample may exhibit multi-modal De distributions, but unlike poorly bleached sediments, these distributions may contain De that tend to both higher and lower apparent doses, obscuring the true burial age (Bateman *et al.* 2007). In the context of Doggerland, this issue is important as bioturbation is a ubiquitous process in shallow marine and estuarine environments (Madsen *et al.* 2010; Reed *et al.* 2006).

***Challenge 3: Mineralogical variations***

Luminescence response is variable between mineral systems, and between minerals of the same system: quartzes and feldspars are characterised by variable brightness and stability of signals. This is quantified as luminescence sensitivity – a measurement of luminescence per unit dose. In the context of Doggerland, this issue is important as mineral response will vary within, and between cores, varying with (and not restricted to) mineral provenance, erosional and depositional histories, and post-depositional diagenesis.

***Challenge 4: Stable dose rate conditions and disequilibrium in uranium decay series***

In routine luminescence applications, secular equilibrium in the decay chains of U and Th through time are assumed, as is 'closed system' behaviour. In 'closed systems', each decay chain tends towards radioactive equilibrium; whereas in 'open systems' exchange of radionuclides, by a variety of physical and chemical processes such as dissolution, sorption and precipitation, can lead to disequilibrium in the decay series, more so for the decay series of uranium (see discussion in Degering and Degering 2020). In many terrestrial settings, it is valid to assume secular equilibrium, and closed system behaviour; but, in marine and near-shore settings this should be not assumed. Surficial deep-sea sediments are known to contain an excess of $^{230}$Th over the series parent $^{238}$U (Armitage and Pinder 2017; Jakobsson *et al.* 2003; Sanderson and Kinnaird 2019), this can decay with depth, and introduce a time dependent component into the dose rate.

Therefore, in the context of Doggerland, in evaluating dose rates to the full range of terrestrial, littoral and marine deposits, anomalies in the concentrations of uranium and/or thorium need to be identified, such that excess activity is quantified and incorporated into dose rate calculations. Moreover, temporal variations in burial conditions need consideration, as the thickness of overburden has implications for the cosmic dose, and fluctuating moisture contents in the sediments will attenuate the external dose.

In addition to the challenges discussed above, there are important, practical considerations when sampling from core materials: a.) there is potential for some light exposure during core retrieval and storage; b.) there is potential for barrel smearing, which could cause additional mixing of sediments (and contributing to further scatter in determined De values) and c.) smaller sample quantities that are obtained from core, compared to sampling from terrestrial sections, necessitate more careful sample preparation and increased counting times. Nelson *et al.* (2019) and Sanderson and Kinnaird (2019) discuss these issues in detail and provide recommendations for secure sampling of subsurface deposits from core in terrestrial and marine settings, respectively.

**Our methodological approach**

***'Solutions' to challenges 1-3***

A number of OSL screening methods have been developed to provide insights into the luminescence properties of sediment and to interpret the depositional mechanisms and zeroing processes. These range from methodological developments such as standardised growth curves (Roberts and Duller 2004), range-finder ages (Durcan *et al.* 2010; Roberts *et al.* 2009) and laboratory profiling (Burbidge *et al.* 2007; Kinnaird *et al.* 2017a; Kinnaird *et al.* 2017b) to instrumentation developments, such as the portable OSL equipment developed at SUERC (Munyikwa *et al.* 2020; Sanderson and Murphy 2010).

In this research, a combination of these approaches was employed: at the time of sampling, luminescence stratigraphies were generated from proxy luminescence data generated with portable OSL equipment (Sanderson and Kinnaird 2019: stage 1). These stratigraphies were 'calibrated', by subjecting sub-samples to laboratory luminescence screening and characterisation measurements, and constructing apparent dose-depth and sensitivity-depth profiles for each core (stage 2). Finally, targeted samples were taken forward to full quantitative quartz SAR OSL dating (stage 3). This approach has several advantages: first, by characterising the 'depositional' sequences for the full length of the core, sampling is better informed and more effective. Second, by generating relative sediment 'chronologies' for the entirety of each core, direct comparisons of sedimentary units down, and between, cores is possible. This provides a means to relate discrete events (e.g. peat inception, inundation) across cores. Moreover, the 'chronology' is not reliant on a small number of dates from arbitrary selected points.

Figure 12.3 illustrates this approach. The examples shown are:

- ELF05B, a length of core 2m long, penetrating *c.* 50cm of grey, laminated silts representing saltmarsh, then brackish mudflats, then *c.* 50cm of grey, fine sands, occasionally speckled with black organic material, attributed to wetland deposition, culminating in peat formation, then tidal access; at 115cm depth in core, till is encountered
- ELF012, a 4m long core of structureless, mid-brown to greyish brown medium- to fine- sands, with common shell fragments and occasional black mottling; there was some debate ahead of sampling as to whether these sediments should be attributed to the Botney Cut Formation (Stoker *et al.* 2011) or if they were a modern sand bank
- ELF022, 6m of alternating medium- and fine-sands, frequently with clay silt laminations, and occasional shell fragments
- ELF054, a length of core 3.8m long, penetrating 2.6m of grey clay silt, with phytal ostracod and clinging foraminiferal fauna suggesting marine-algae and/or seagrass, in a brackish lagoon, then 1.1m of silts (10cm thick) interbedded with dark brown fibrous peats (*c.* 50cm thick)

Figure 12.3a shows how breaks, or step changes, in IRSL and OSL net signal intensities might indicate where discontinuities, or unconformities, are present in the core stratigraphies. This was observed when sampling ELF005B: net signal intensities drop off through units 5B-3, -4 and -5, approaching the transition from brackish lagoon to wetland deposition. (The inverted signal-depth progression through 50 to 64cm tracks a reduction in grain size through the same interval, and an increased prevalence of wavy, sub-parallel clay-silt laminations). Across the 5B-5/-6 transition, there is a substantial step-change in intensities, across an order of magnitude, which attests to this boundary representing a considerable amount of time. The subsequent calibrated laboratory analyses provide some quantification to this: the break corresponds to 20Gy.

Figures 12.3b and 12.3c show how signal-depth progressions can provide insights on rates of sedimentation: consistent signal intensities with depth might indicate high rates of sedimentation (Figure 12.3b), whereas, slow, steady signal-depth progression likely represents a slow rate of sedimentation (Figure 12.3c). The range in intensities across these progressions provides the relative rate of sedimentation. With ELF012, we concluded during sampling that the range in signal intensities observed across the 6m length of core suggested that these sands had accumulated rapidly. Moreover, as there was no distinction between the signal intensities at the very top of the core (i.e. modern sands) and those at 6m depth, that these sands are modern and represent a sand bank on the seabed. In contrast, in ELF022, between 50 and 80cm depth in core, there is a steady increase in signal intensities with depth, implying a slower and more steady sedimentation across this interval.

Finally, Figure 12.3d, illustrates how the amalgamation of all proxy luminescence data (together with sedimentological observations, and when available other environmental proxies (e.g. Allaby *et al.* this volume; Bates *et al.* this volume) provides temporal (and spatial) frameworks to aid interpretation of the depositional sequences and histories. It demonstrates that: a.) the marine sands encountered through 0.00 and 0.88m depth in core are stratified, with some chronology, which led to re-appraisal of this unit, and the recognition that this was more than a recent sand wave; b.) through 0.88 to 1.25m, and then 1.25 to 1.45m, IRSL and OSL signal intensities track a reduction in silicate content, with implications for reconstructing dosimetry; c.) through 1.45 to 2.60m, intensities increase with depth, which notwithstanding b.) implies a considerable chronology across this interval on the order of ×2-5; and d.) that the till encountered at 2.85m was reworked to a depth of 15-20cm, during deposition of the overlying unit.

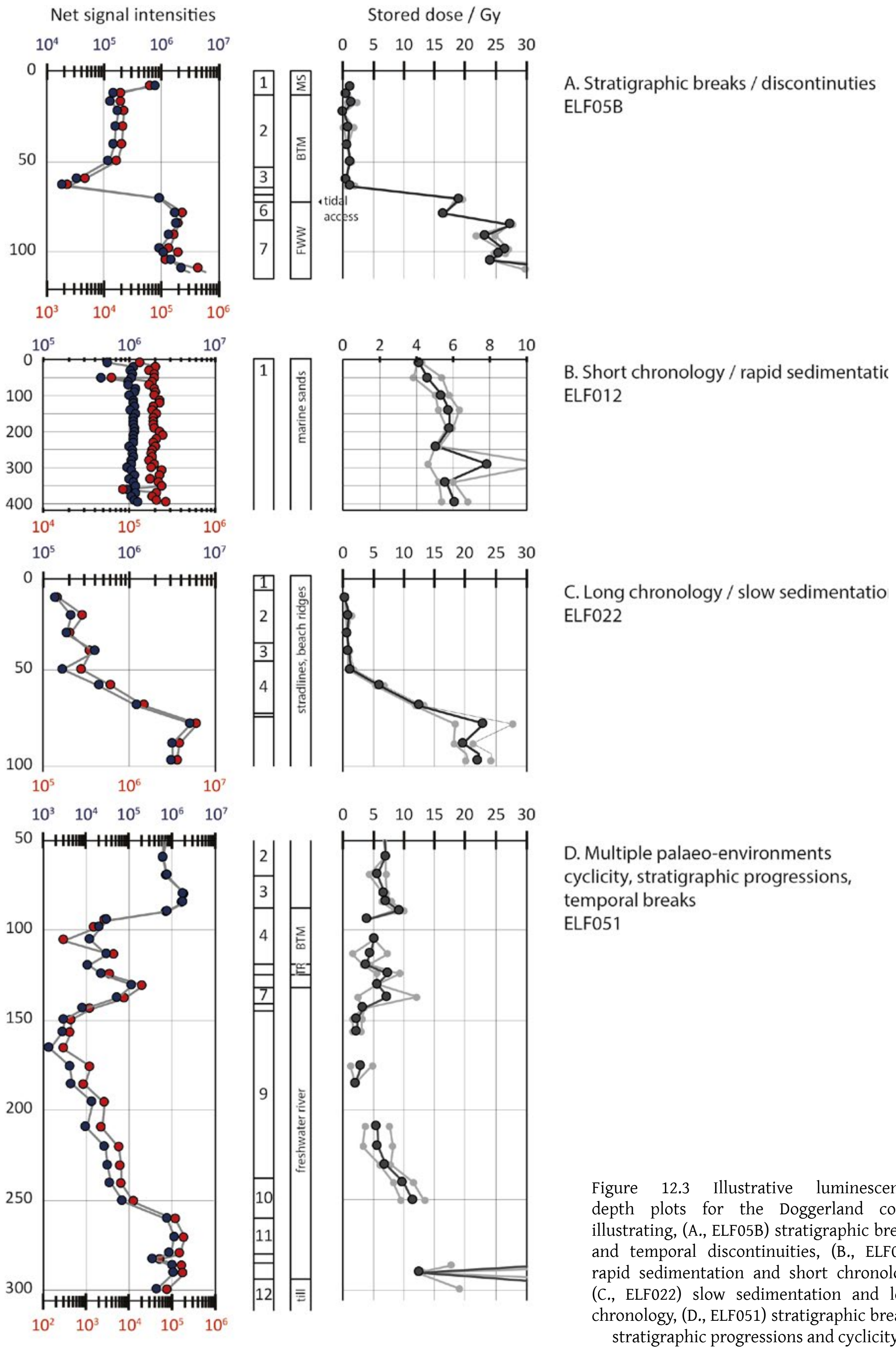


Figure 12.3 Illustrative luminescence-depth plots for the Doggerland cores: illustrating, (A., ELF05B) stratigraphic breaks and temporal discontinuities, (B., ELF012) rapid sedimentation and short chronology, (C., ELF022) slow sedimentation and long chronology, (D., ELF051) stratigraphic breaks, stratigraphic progressions and cyclicity.

Therefore, only samples with promise are selected for luminescence dating, maximising the chances of success for dating. When more challenging samples were sampled, and partial bleaching or post-depositional sediment mixing were identified as issues, statistical techniques examining the degree of over-dispersion in De and the measure of skewness and kurtosis in De distribution were examined (Galbraith *et al.* 1999; Olley *et al.* 1998).

**Application to the *Europe's Lost Frontiers* Project**

*Europe's Lost Frontiers* is investigating the submerged landscape of Doggerland, reconstructing it's palaeoenvironments through extensive marine survey and sediment coring (Gaffney and Fitch this volume); with the sediment cores subjected to detailed sedimentological, palaeoenvironmental (Bates *et al.* this volume), geochemical (Bensharada *et al.* this volume; Finlay *et al.* this volume) and sedimentary ancient DNA (Allaby *et al.* this volume) analysis.

OSL and radiocarbon dating (Hamilton *et al.* this volume) provide the chronologies to underpin these studies.

78 cores from 60 locations have been collected, of which 40 have material of interest; 22 of these have been sampled for OSL profiling and dating. The recovered materials in these cores are from a range of palaeo-environments, including marine sands, intertidal muds, brackish lagoons, peats (from a few centimetres thick to 1.8m), lakes, rivers and palaeosols (Figure 12.2).

The methods and protocols employed in luminescence dating, as applied in the *Europe's Lost Frontiers* project, are illustrated with reference to core ELF001A. Core ELF001A is significant to palaeo-environmental reconstructions of Doggerland, as its sedimentary sequences preserve a proxy record of final submergence of Doggerland, and potentially encloses materials related to the Storegga Tsunami (Gaffney *et al.* 2020).

Borehole ELF001A is located at the head of a palaeo-river system near the Outer Dowsing Deep (the Southern River, Fitch *et al.* this volume: Chapter 6). Prior to final submergence, with the majority of the landscape already lost to sea-level rise, the surviving land would have been low lying and close to sea level. This landscape would have been vulnerable to catastrophic flooding events. A key regional event during this period was the Storegga Tsunami, which occurred in response to a series of underwater landslides off of the Norwegian coasts 8.15 thousand years before present. This tsunami hit the eastern Scottish and English coastlines, and likely reached the southern North Sea. Some workers (Bondevik *et al.* 2012; Fruergaard *et al.* 2015; Weninger *et al.* 2008) have suggested the Storegga Tsunami led to the final abandonment of the island by Mesolithic communities.

Seven lithological units were identified within this core: units 1A-1 to 1A-3, consist of sands or sandy gravels with marine shells; units 1A-4, well-laminated fine-grained sandy silts; unit 1A-5, a thin sequence of silty sands with broken shell fragments; unit 1A-6, well-laminated sands and silts, overlain by poorly sorted sands and shell detritus; unit 1A-7, well-laminated fine-grained sandy silts. Modern or recent mobile bottom sands are represented by units 1A-1 to 1A-3 and have not been sampled or considered in any detail.

Estuarine mudflat conditions are represented in the core in units 1A-4 and 1A-7, which are interrupted by coarse poorly sorted shelly gravel (1A-5/1A-6). The mixture of marine and brackish material alongside broken and fragmentary shell remains, and common small clasts, suggests these sediment units represent a high-energy event intruding into otherwise sheltered mudflat environments Further multi-proxy data from ELF001A, as reported in Gaffney *et al.* (2020), provided evidence to suggest that these units were the deposits of the Storegga Tsunami.

**Methodological details**

***Stage 1 – Preliminary OSL screening of cores***

For the subset of sedimentary cores selected for OSL investigation, the sedimentological and geophysical evidence were reviewed, and the key stratigraphic intervals and depths of interest noted. Cores were split under subdued light conditions at the University at Warwick, with one half retained there for sedaDNA analyses, and the other transferred to the University of Wales Trinity Saint David, Lampeter campus, for sedimentological and luminescence investigation. At Lampeter, the cores were subsampled for luminescence screening using portable OSL equipment (Munyikwa *et al.* 2020).

The protocol adopted throughout the study was as follows:

1. through each core, sediment was extracted at regular 10cm intervals, with tighter resolution sampling at stratigraphic and lithological boundaries (and if available, prominent breaks in the geochemical data; Figure 12.4)
2. these sub-samples were immediately measured using a SUERC portable OSL reader, using an interleaved sequence of system dark-count, IRSL and OSL (cf. Sanderson and Kinnaird, 2019)
3. from this, IRSL and OSL net signal intensities and IRSL and OSL depletion indices were calculated

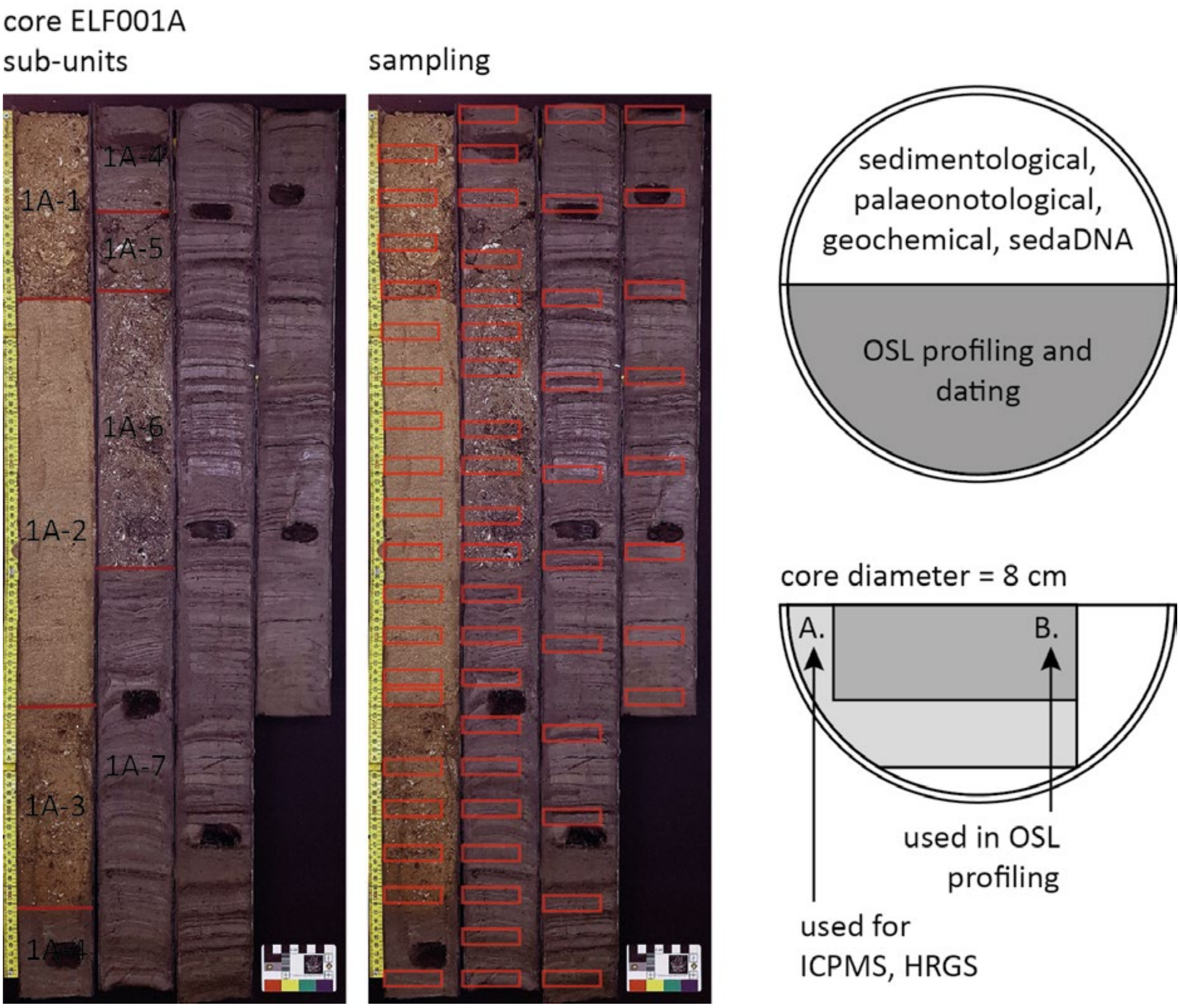


Figure 12.4 Sampling strategy for ELF cores – illustrated with core ELF001A: (a) core, with sub-units identified; (b) core, with sampling positions indicated; (c) removal of sediment for OSL profiling, OSL dating and dosimetry.

for all samples, and luminescence-depth profiles generated for each core (Figures 12.3 and 12.5)

4. this, in combination with sedimentological observations and the expectations of dating, were used to position samples for quantitative quartz OSL dating
5. for the positions in the core selected for dating, larger samples were taken from between the profiling samples, and associated samples collected for dosimetry

Using this approach, the 22 investigated cores were appraised through more than a thousand samples, which permitted the construction of high-resolution luminescence 'stratigraphies'. IRSL and OSL signals were readily detectable in all cores, confirming that phases suitable for luminescence dating were present. IRSL signal intensities range from 120 to $1.83 \times 10^7$ counts; and excluding the more organic rich horizons in ELF002, 005B, 034, 051, 054, from 5160 counts. Peats and very-organic rich silts were not sampled for OSL. OSL signal intensities range from 1440 to $1.57 \times 10^8$ counts; and excluding the more organic rich horizons, from $2.29 \times 10^4$ counts. IRSL and OSL depletion indices range between 1.09 and 3.03, and 1.09 and 3.17, respectively. The dynamic range in IRSL signal intensities observed down individual cores is at least one order of magnitude (41% of investigated cores), and commonly more (2 orders, 36%; 3 orders, 18%; 4+ orders, 5%); similar dynamic ranges were observed in OSL net signal intensities (1 × 10, 32%; 2, 45%; 3, 18%; 4+, 5%).

Luminescence responses, therefore, vary down core, and clearly record mineralogical, luminescence age, sensitivity and dosimetry variations.

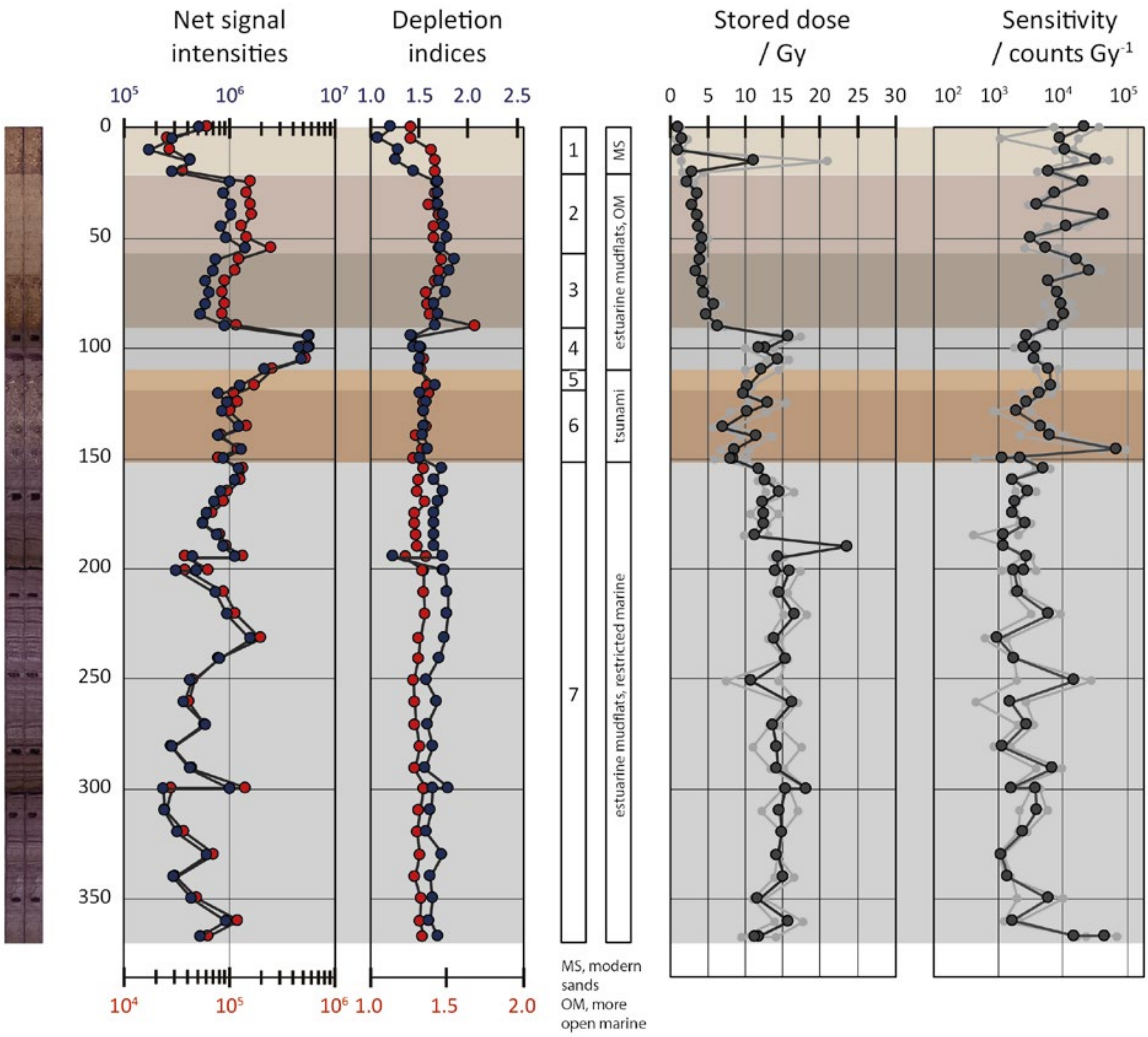


Figure 12.5 Illustrative luminescence-depth plots for ELF001A: on the left, IRSL and OSL net signal intensities and depletion indices; on the right, apparent dose and sensitivity distributions.

*To illustrate this, we use the example of ELF001A. Figure 12.5a shows the proxy luminescence stratigraphies relative to the lithostratigraphy of the core, through units 1A-1 to 1A-7. Observations, and inferences from these, are tabulated in supplementary data. From 0 to 21cm depth, the sands are characterised by fluctuating OSL signal intensities in the range 1.75 to 5.30 × $10^5$ counts, with no stratigraphic coherence, and low depletion indices, <1.3. Together, this data suggests that these sands are modern and mobile. The trend in fluctuating OSL signal intensities with depth continues through 21 to 67cm, although across a greater range, 7.08 × $10^5$ to 1.44 × $10^6$ counts. From 67 to 90cm depth, there is a slight signal-depth progression from 6.01 × $10^5$ to 9.26 × $10^6$ counts, and depletion indices are higher than observed in unit 1A-1. The step change in OSL intensities across the unit 1A-1 / 1A-2 boundary, then the signal-depth progression in unit 1A-3, all suggest that units 1A-2 and 1A-3 record some chronology and stratigraphy is preserved.*

*From 90 to 109cm, unit 1A-4, there is an inverted signal-depth progression from 5.71 to 4.96 × $10^6$ counts, and the lowest depletion indices observed in the core aside from unit 1A-1. The step-change in OSL intensities across the unit 1A-3 / 1A-4 boundary implies that the sediment has a difference provenance. The low depletion indices suggest that this material is poorly bleached, and that the composite OSL signals include residuals.*

*Between 109 and 151cm depth, units 1A-5 and 1A-6, the luminescence profiles are more complex: with 'couplets' on the scale of 4 to 5cm, characterised by both normal and inverted signal-depth progressions. Interestingly, in each 'couplet' the lower signal intensities correlate with higher depletion indices. The 'cyclicity' in OSL intensities and depletion indices is interpreted here as reflecting deposition from multiple waves: the first influx of sediment is characterised by low OSL intensity and high depletion index; then, higher intensities and lower depletion indices. The first wave is well-bleached and characterised by low intensities and high depletion indices, then the subsequent waves, are only partially bleached and characterised by high intensities and low depletion indices. It is notable that across the 'couplets', signal intensities vary over a similar magnitude and range, suggesting a common provenance.*

*From 155 to 180cm, signal intensities drop from $1.24 \times 10^6$ to $5.78 \times 10^5$ counts, before increasing with depth through the interval 180 to 200cm, from $5.78 \times 10^5$ to $1.16 \times 10^6$ counts, from 200cm to depth, signal intensities remain relatively consistent at approximately $1.59 \times 10^6$ counts. This implies that unit 1A-7 should be further sub-divided into two sub-units 1A-7a and 1A-7b and illustrates for this interval that screening at sampling can identify crypto-stratigraphic boundaries.*

Having shown that there are readily measureable IRSL and OSL signals, and that these signals vary with stratigraphy down core, the investigations progressed to laboratory analysis, first to calibrated luminescence screening and characterisation (stage 2), then to full quartz SAR OSL dating. The 'calibrated' profiles as obtained in stage 2 (below), remove some of the ambiguity in interpreting the relative 'luminescence stratigraphies', relating to bulk mineral properties (mineralogy, grain size, sensitivity, colour etc).

***Stage 2 – OSL calibration and characterisation of cores***

Sample preparation and laboratory analyses were undertaken in the luminescence laboratories of the School of Earth and Environmental Sciences (SEES), University of St Andrews. This stage in the methodology is to characterise a sub-set of the profiling samples in the laboratory, to provide a first approximation of the magnitude and range in luminescence sensitivities and apparent (or burial) doses. OSL measurements were carried out using Risø TL/OSL DA-15 and DA-20 automated dating systems. Full technical details of the SEES instruments are provided in García *et al.* (2019).

The protocol adopted here, was as follows:

1. sub-samples from the initial luminescence profiling were subjected to simplified mineral separation procedures (cf. Sanderson and Kinnaird 2019: supplementary data)
2. paired aliquots of HF-etched from each sub-sample were subjected to a simplified SAR OSL protocol for a preliminary assessment of apparent dose (cf. Sanderson and Kinnaird 2019); The readout cycle consisted of: a.) a preheat at 220°C, held for 10s; b.) OSL at 125°C for 60s, c.) a test-dose of 1Gy, d.) a preheat of 220°C, e.) OSL at 125°C for 60s, f.) then, repeats of steps a.) to e.) following regenerative doses of nominal doses of 10, 30, 60Gy (extended to 120Gy, when necessary) and 0Gy. The zero dose was omitted from the readout cycles of ELF003, 005B and ELF031A. A recycling dose of 10Gy was added to the readout cycles of at least one length of core from ELF001A, 007, 019, 022, 027, 034, 039, 054 and 059
3. from this, the distributions in sensitivities and apparent dose were calculated, and plotted vs depth in core
4. these plots were used to test the assumptions made during initial profiling and to re-appraise the most promising targets for dating

906 of the 1104 preliminary samples were taken forward to further laboratory analyses (this equates to 82% of the dataset).

From this, we obtained the first indication of bulk mineral / luminescence behaviour, which were promising: OSL sensitivities ranged from 110 to $1.48 \times 10^6$ counts Gy-1. 81% of aliquots returned an OSL sensitivity >1000 counts $Gy^{-1}$ and, 91% of aliquots, a sensitivity >500 counts $Gy^{-1}$. Recuperation was, in general, low with a mean value of 6.7 ± 11.0 % (error expressed here, and elsewhere, as standard deviation); 66% of aliquots returned a recuperation value <5%. Recycling ratios were, in general, good with a mean of 1.04 ± 0.35; with 82% of aliquots returning recycling ratios within ± 0.1 error of unity. By substituting the 1st regenerative dose for the natural dose in each dependent SAR curve, and comparing this nominal normalised value to the known given dose, pseudo-dose recovery 'ratios' are obtained for each sample. The mean value for pseudo-dose recovery was 1.07 ± 0.26.

OSL apparent doses ranged from 0.1 to >100Gy; relatively few aliquots returned apparent doses in the sub-Gy region (<4%), and <7% returned apparent doses in excess of 60Gy. With the exception of ELF012, the dynamic range in apparent doses down core is in the range of $10^2$ to $10^3$, which attests to long sediment chronologies and moreover the preservation of stratigraphy in these cores (which partly addresses challenge 2: post-deposition sediment mixing). These analyses suggest the cores, and/or parts of the cores, where apparent doses are low and likely to return early Holocene depositional ages, and where apparent doses are high, which in a low dose rate environment would correspond to late Pleistocene and earlier dates. Earlier, with reference to the luminescence stratigraphies shown in Figure 12.3, we suggested the parts of cores ELF012 and ELF022, where we might expect sedimentation to be slow and gradual, or episodic and rapid. Both these trends are reproduced in the calibrated laboratory dataset. Across the 6m length of core in ELF012, the progression in apparent doses is from 4 to 5Gy; whereas for the 20cm thickness of unit 22-4 in ELF022, apparent doses increase from 6 to 22Gy. With any estimate of environmental dose rate, this implies that the sediments in ELF012 represent a short chronology (and rapid deposition), whereas, a considerable chronology (and slow sedimentation) is represented in ELF022.

*The detail in this is illustrated using the example of ELF001A. All 61 samples from this core were taken forward to preliminary laboratory characterisation. As before, key observations, and inferences from these, are tabulated in supplementary data.*

*Unit 1A-1 is characterised by variable OSL apparent doses in the range 0.7 to 1.7Gy (with one high dose outlier, trending to in excess of 20Gy), with poor paired reproducibility between aliquots, and no stratigraphic coherence. The sensitivity distribution is also heterogeneous, varying across two orders of magnitude.*

*In contrast, units 1A-2 and 1A-3 show a progression in OSL apparent doses with depth, through 21 to 90cm, from 1.7Gy to 5.7Gy. The paired reproducibility between aliquots is good: apparent doses reproduce within error between 30 and 55cm and 70 and 85cm. The sensitivity distribution is less heterogeneous, varying across a single order of magnitude. This supports the hypothesis raised at sampling: unit 1A-1 is modern and mobile, units 1A-2 and 1A-3 record some chronology and stratigraphy is preserved.*

*Across the unit 1A-3 / 1A-4 boundary, there is a step increase in OSL apparent doses, from 5.7Gy to in excess of 10Gy. Even withstanding large variations in environmental dose rate across this boundary, this attests to a large temporal break between these units. From 90 to 109cm, apparent dose estimates are inverted, from c. 14 to 10Gy. The fine-grained sandy silts of unit 1A-4 are characterised by lower luminescence sensitivities than the coarser-grained sands of units 1A-1 to 1A-3. In the original interpretation, it had been assumed that the step-change in net signal intensities across the boundary reflected a change in provenance; but the lower signal intensities returned from unit 1A-4 reflect in part the lower sensitivities of these sediments.*

*The sensitivity and apparent dose distributions for units 1A-5 and 1A-6 are complex, varying on the 5 to 10cm scale: between 109 and 119cm, apparent dose values are consistent at c. 10Gy, with good paired reproducibility; from 121 to 129cm, apparent doses show a normal dose-depth progression, from 9.5-10Gy to >12Gy, with poor reproducibility between aliquots; from 136 to 146cm, some scatter is noted in apparent doses, which vary between 6 and 13Gy; from 150 to 155cm, apparent dose values are consistent at c. 8Gy. Paired reproducibility is variable: although the lower doses in each couplet show better paired reproducibility (varying within 10%), and the higher dose outliers in each, poorer reproducibility (diverging by up to 50%). There are several interpretations to this, successive waves may have entrained more 'old' sediment as they moved inland, or alternatively, 'old' buried and un-zeroed sediment from deeper water and/or beach were sequentially cut into and entrained by later waves. In either scenario, zeroing of the luminescence signals during tsunami-transport was variable, from partial to good.*

*Across the unit 1A-6 / 1A-7 boundary, there is a step increase in apparent dose values to 10 to 13Gy, consistent with a temporal break. From 200cm depth in core, there is another step-increase in apparent doses to values fluctuating around 14.5Gy. This corroborates the hypothesis raised at sampling of a lithostratigraphic division in unit 1A-7 that must correspond to a change in depositional conditions.*

This stage of the investigations provided the further temporal (and spatial) frameworks for each of the investigated cores, providing insights on the depositional histories, and indicating the parts of the cores, and units, amenable for OSL dating. Subsequent to this, the luminescence stratigraphies were reviewed, dating priorities discussed with colleagues in the *Europe's Lost Frontiers* team, and targets/sedimentary units identified for OSL dating.

***Stage 3 – Quantitative quartz SAR OSL dating***

Dating priorities differ from core to core, covering deposits from a range of palaeo-environments from mudflats, estuarine mudflats to terrestrial shorelines and fluvial deposits (Figure 12.2).

In regard to reporting luminescence ages in this, and subsequent volumes in the *Europe's Lost Frontiers* monograph series, the data generated during all stages will be appended to the relevant chapter. The supplementary data will be reported in the following format: 1. luminescence stratigraphies; 2. representative decay and dose response curves; 2. equivalent dose determinations/distributions; 4. dose rate determinations; and 5. OSL depositional ages, with a commentary on geomorphological and/or palaeo-environmental significance.

***Equivalent dose determinations***

Standard mineral preparation procedures as routinely used in OSL dating were used to extract sand-sized quartz from each sample (cf. Kinnaird *et al.* 2017a, 2017b). Further technical details are provided in supplementary data. Variable quartz yields necessitated the need to explore several grain size fractions, typically 90-150 and 150-250µm.

Equivalent doses (De) were determined by OSL using a single aliquot regenerative dose (SAR) OSL protocol (cf. Murray and Wintle 2000; Sanderson and Kinnaird 2019: supplementary data).

Quartz from the *Europe's Lost Frontiers* cores was characterised by a range of responses, reflecting regional variations in lithofacies, mineralogy and depositional setting. As standard in the SAR OSL protocol, individual aliquots, or equivalent doses were only taken forward to analysis if they passed strict SAR acceptance criteria: a.) Sensitivities had to exceed >1000 counts per Gy; b.) Recuperation had to be < 10% of the natural signal (it was typically < 5%); c.) Recycling ratios had to be within 10% of unity; d.) pseudo-dose recovery ratios had to be within 10% of unity and/or e.) aliquots had to show no significant IRSL response associated with anomalous equivalent doses.

In general - and as observed in the exploratory laboratory dataset - the *Europe's Lost Frontiers* quartz was responsive to SAR OSL: approximately 70% of measured aliquots passed SAR acceptance criteria. Mean sensitivities were in the range 3400 ± 260 and 3650 ± 520 counts $Gy^{-1}$, for the 150-250µm and 90-150µm grain size fractions, respectively. Recuperation remained low, 6.2 ± 5.3 and 4.2 ± 2.2 %. Recycling ratios were within error of unity, 1.02 ± 0.02 and 1.02 ± 0.03, as were pseudo-dose recovery ratios, 0.99 ± 0.02 and 1.00 ± 0.03. IRSL response was variable, with mean responses of 17.4 ± 20.0 and 18.4 ± 28.1%, but equivalent dose varied independently of IRSL response.

Unsurprisingly, equivalent dose distributions were variable, with depositional setting and bleaching potential, contributing to dispersion in De values. Discrete equivalent dose distributions were appraised for homogeneity, and, where stratigraphic associations are established, different combinations of merged datasets explored. Average values of over-dispersion were 30.9 ± 17.5 and 32.3 ± 20.3 % for the 150-250 and 90-150µm fractions respectively.

***Dose rate determinations***

Activity concentrations of potassium, uranium and thorium were estimated from high-resolution gamma spectrometry (HRGS) measurements, conducted at the Environmental Radioactivity Laboratory at the School of Biological and Environmental Sciences, University of Stirling, and inductively-coupled plasma mass spectrometry (ICPMS), at the StAiG laboratories at the School of Earth and Environmental Sciences, University of St Andrews and at Activation Laboratories, Canada. For a number of cores, semi-quantitative element concentrations of K, U and Th as obtained by X-ray Fluorescence core scanning where available down-core. Core scanning by X-ray Fluorescence was undertaken at Aberystwyth University.

These data were used to determine infinite matrix dose rates for alpha, beta and gamma radiation, using the conversion factors of Guérin *et al.* (2011), grain-size attenuation factors of Mejdahl (1979) and attenuated for moisture content. 'Fractional water' values, ranged between approximately 8 and 40% of dried weight (mean, 23 ± 7%; n= 129), and 'saturated' values, between 12 and 50% of dried weight (mean, 30 ± 11%).

The Doggerland samples had, in general, low activity with K, U and Th concentrations ranging between 0.2 and 3.1%, 0.2 and 8.4ppm and 0.6 and 15.40ppm, respectively (with mean values of 1.5 ± 0.6 % K, 1.7 ± 1.2ppm U and 5.6 ± 3.5ppm Th; n = 132). The ratio of Th:U ranged between 1.07 and 7.05, with a mean of 3.4 ± 0.9; approximately 80 % of the samples measured returned typical Th:U ratios, 3.2 ± 0.5 (n = 103). For the 29 samples with atypical Th:U ratios, further investigations have been instigated to explore disequilibrium in the uranium decay series and determine time-dependent dose rates. These samples have not been taken forward to dating and are excluded from further discussion.

Beta dose rates from HRGS were in the range 0.9 to 1.1mGy $a^{-1}$; and from ICPMS, 0.4 to 2.5mGy $a^{-1}$, with a mean estimate of 1.2 ± 0.5mGy $a^{-1}$. Wet gamma from HRGS were in 0.5 to 1.0mGy $a^{-1}$; and from ICPMS, 0.2 to 1.6mGy $a^{-1}$, with a mean estimate of 0.6 ± 0.3mGy $a^{-1}$.

The contributions from the cosmic dose were modelled after Sanderson and Kinnaird (2019), by combining latitude and altitude specific dose rates (0.17 ± 0.01mGy $a^{-1}$), with time-dependent corrections for water depth and overburden (for the period the terrestrial sediments accumulated). Consideration was given to the palaeo-environment(s) of deposition: a.) for sediments sampled from shallow-marine to offshore deposits, the depth of water above the deposit would have attenuated the cosmic dose contribution to a few percent of the total dose; b.) similarly, for the shoreline and nearshore deposits rapidly flooded in inundation (100s of years), the contribution as percent would be low; c.) it is only for the terrestrial deposits, that the cosmic dose contribution needed to be modelled.

Total environmental dose rates to the 90-150µm, HF-etched quartz were in the range 0.7 to 3.3mGy $a^{-1}$, with a mean estimate of 1.8 ± 0.7mGy $a^{-1}$.

***Age determinations***

Depositional ages were calculated for discrete depths in each core using standard micro-dosimetric models, with uncertainties that combined measurement and fitting errors from the SAR OSL analysis, dose rate evaluation uncertainties, and allowance for the calibration uncertainties of the sources and reference materials.

In each core, consideration was given to:

1. the luminescence stratigraphies generated at sampling, and the stratigraphic progressions and/or temporal breaks implied
2. the sensitivity and apparent dose distributions determined during preliminary laboratory analysis
3. the equivalent dose distributions obtained at discrete depths, which were appraised for homogeneity
4. the combined distributions from across lithostratigraphic units, which were appraised for homogeneity, when the luminescence profiles suggested stratigraphic coherence. Different permutations of the assimilation of equivalent doses to obtain the burial dose were also considered, including weighted combinations and statistical dose models (Guérin *et al.* 2017)
5. the variations in radionuclide concentrations down core, the gradients and/or breaks in dosimetry, and in estimating environmental dose rates to the positions of the dating samples
6. depositional ages, which were calculated for discrete units, and when considerations 1 to 5 suggested stratigraphic coherence, conventional statistical and/or Bayesian approaches used to assimilate depositional ages for stratigraphic units and/or events

*To illustrate this, we return to the example of core ELF001A. The dating priorities identified in this core were: 1.) the top of unit 1A-7 (at 155cm depth), well-laminated fine-grained sandy silts deposited under estuarine mudflat conditions; 2.) the base of unit 1A-6, the 'tsunami' deposit (at 151cm); 3.) the base of unit 1A-4, well-laminated fine-grained sandy silts deposited under more open marine estuarine mudflat conditions (at 108cm).*

*Thirteen sub-samples from across these stratigraphic units were taken forward to dating: four of these were from the top of unit 1A-7 at depths in core of 155, 160, 170 and 190cm; a further four were taken through unit 1A-6 at depths of 136, 140, 146 and 150cm; two from unit 1A-5 at depths of 110 and 117cm; and four from unit 1A-4 at depths of 95, 100, 100 and 105cm.*

*Figure 12.6 presents the equivalent dose distributions as Abanico plots for units 1A-4, -5, -6 and -7. Given the evolving depositional environment from estuarine mudflat to high-energy marine, to estuarine mudflat, a range of responses were expected: but fortuitously, the equivalent dose distributions showed reasonable homogeneity, and good internal consistency. Values of overdispersion ranged between 10.3 and 37.3 %, with a mean of 20.5 ± 8.3 %. The samples with the most pronounced heterogeneity, were those located close to lithological boundaries and / or transitions in palaeo-environments (i.e. top of unit 1A-7, immediately beneath tsunami deposit = 37.3 %; base of unit 1A-5 = 33.7%). Table 12.1 lists the apparent dose estimates (90-150µm) determined for discrete depths down-core in ELF001A (these were calculated using a central dose model in the R package luminescence). The apparent dose estimates for the 90-150 and 150-250µm fractions are shown relative to each other in Figure 12.7.*

*The apparent dose values correlate well with the apparent dose-depth profile obtained for ELF001A ($R^2$ = 0.943).*

*Down-core variations in radionuclide concentrations for ELF001A are shown in Figure 12.8, together with the estimates of the environmental dose rate to the HF-etched, 90-150µm quartz fractions. Unsurprising given the contrasting lithologies and diverse environmental conditions, radionuclide concentrations vary with position in core: the highest concentrations observed in K, Th and U are from the estuarine mudflats, both at the base of unit 4 and the top of unit 7 (> 1.5 % K, >3.5 Th ppm, > 1.7 U ppm); concentrations drop off through unit 5 of the tsunami deposit (from 1.3 to 0.8 % K, 5.6 to 4.3ppm Th, 1.8 to 1.2 U ppm); and are lowest in unit 6 of the same deposit (min 0.8 % K, 2.5 Th ppm, 0.8 U ppm). K, U and Th concentrations are most variable in unit 6. Throughout, Th:U ratios remain typical at 3.2 ± 0.7.*

*Total environmental dose rates vary down core: unit 4, comprising the estuarine mudflats with open marine affinities, is characterised by dose rates in the range 1.5 to 2.7mGy $a^{-1}$; unit 5 of the tsunami deposit by dose rates in the range 1.0 to 1.4mGy $a^{-1}$; unit 6 of the same deposit, 1.0 to 1.5mGy $a^{-1}$; and unit 7, 1.8 to 2.2mGy $a^{-1}$.*

*Individual sediment ages range from 9.2 ±1.4 ka at the top of unit 1A-7, to between 8.3 ±1.1 ka to 7.9 ±0.5 ka within units 1A-5 and -6, to 7.2 ±0.5 ka immediately above (base of unit 1A-4); with statistical combinations suggesting depositional ages for units 1A-5 and -6 between 8.0 to 8.2 ka (Table 12.2). The combined age of 8.14 ± 0.29 ka for units 1A-5/-6 is consistent with the hypothesis suggested above that these are tsunami deposits related to the Storegga Slide. Final inundation of Doggerland in the position of this core did not occur to 7.16 ± 0.50 ka, and together with the multi-proxy evidence from ELF001A, this shows that the landscape temporarily recovered after the Storegga tsunami.*

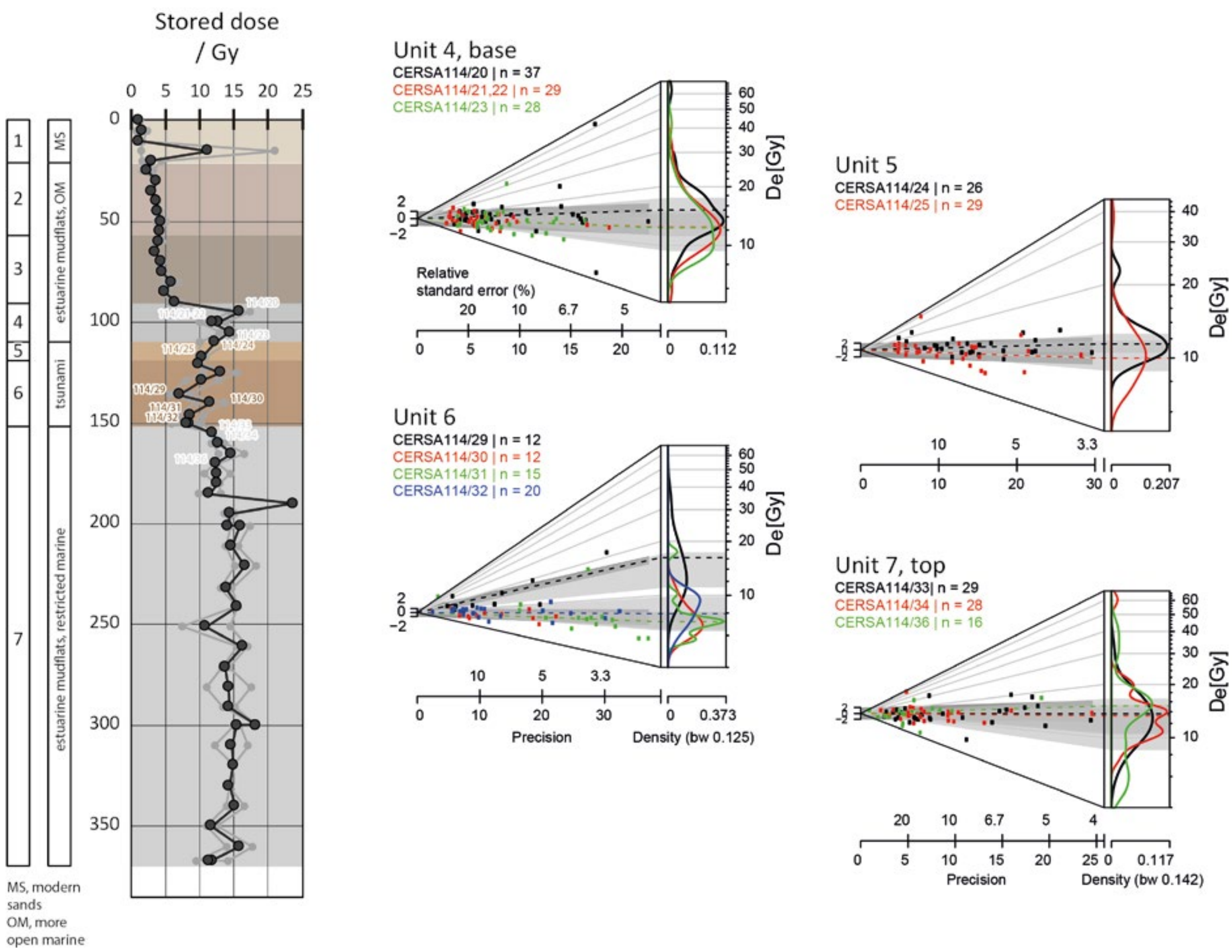


Figure 12.6 De distributions for ELF001A, 90-150µm, shown relative to the stratigraphy of the core. Units for ELF001A as discussed in the text.

<table>
<tr><th>CERSA ID</th><th>Depth /cm</th><th colspan="2">Unit</th><th>Apparent dose / Gy</th></tr>
<tr><td>114/20</td><td>95</td><td colspan="2" rowspan="4">Unit 4, estuarine mudflats</td><td>8.36 ± 0.53</td></tr>
<tr><td>114/21</td><td>100</td><td>15.60 ± 1.07</td></tr>
<tr><td>114/22</td><td>100</td><td>12.74 ± 0.40</td></tr>
<tr><td>114/23</td><td>105</td><td>12.55 ± 0.72</td></tr>
<tr><td>114/24</td><td>110</td><td rowspan="2">5</td><td rowspan="6">Tsunami</td><td>11.45 ± 0.32</td></tr>
<tr><td>114/25</td><td>117</td><td>10.66 ± 0.89</td></tr>
<tr><td>114/29</td><td>136</td><td rowspan="4">Unit 6</td><td>13.34 ± 0.99</td></tr>
<tr><td>114/30</td><td>140</td><td>7.19 ± 0.31</td></tr>
<tr><td>114/31</td><td>146</td><td>7.48 ± 0.66</td></tr>
<tr><td>114/32</td><td>150</td><td>8.30 ± 0.35</td></tr>
<tr><td>114/33</td><td>155</td><td colspan="2">7, EM-RM</td><td>15.14 ± 1.81</td></tr>
</table>

Table 12.1 Stored dose estimates for the 90-150μm quartz fractions from ELF001A (lab code, CERSA114).

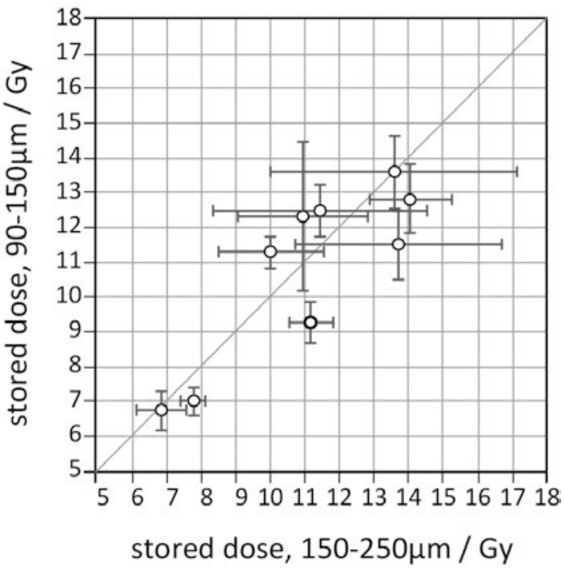


Figure 12.7 Stored dose estimates for the 90-150μm and 150-250μm quartz fractions.

**Discussion**

As demonstrated through core ELF001A, work progressed successively through a three-staged approach, from initial screening of the core stratigraphies at sampling (stage 1), through calibrated characterisation of these stratigraphies in the laboratory (stage 2), towards final quartz SAR OSL dating (stage 3). Through OSL, a chronology and sedimentation history were established for early to mid-Holocene deposits in this core, providing a temporal framework to pin palaeo-environmental interpretations and reconstructions.

This demonstrates the potential of OSL for dating the ELF core sediments. It also illustrates the added value in contextualising the luminescence stratigraphy across the entirety of the core, and how stratigraphic breaks and progressions aid in interpreting depositional sequences and histories. At the broad scale, the calibrated datasets show the cores, and/or parts of cores, where apparent doses are low, suggesting that for these units/intervals, the sediment is likely to return later Holocene dates. Larger apparent dose estimates, which in a low dose rate environment would correspond with substantially older dates, potentially record late Pleistocene ages. At a higher resolution, intricate fluctuations in apparent doses and sensitivities with depth: 1.) inform on sedimentation rates, 2.) suggest the chronology to the unconformities and hiatuses identified in the cores, and 3.) provide temporal (and spatial) frameworks to aid sedimentological and palaeoenvironmental interpretations. Through, a critique of this data, we are able to select the units and/or parts of the cores which hold most promise for dating, mitigating the challenges associated with partial bleaching, bioturbation, and other depositional and environmental conditions (challenges 1 to 4 above).

In further justification of this approach, the apparent doses obtained through preliminary laboratory characterisation broadly correlate with the apparent dose estimates obtained in full quartz SAR OSL dating (Figure 12.9a). There is a degree of variability down-core, and also between cores, but this is unsurprising given the range of lithologies sampled.

The final phase of OSL investigations on the ELF cores from Doggerland is still ongoing. At the time of print, 103 samples have been subjected to full quantitative quartz SAR OSL, providing temporal constraints on final inundation of Doggerland, and the early Holocene and late Pleistocene palaeo- environments and geographies (Figure 12.9b). This includes new constraints on inundation: at the position of core ELF001A, inundation was complete by 7.16 ± 0.50 ka; at ELF003, inundation is dated to between 7.93 ± 1.11 to 7.21 ± 0.98 ka, most probably at 7.71 ± 0.51 ka; and at ELF022, between 8.33 ± 0.91 and 7.37 ± 0.73 ka, with weighted combinations suggesting inundation by 7.84 ± 0.42 ka. For ELF045, a *terminus post quem* is provided by the end of tidal mudflat accumulation at 8.19 ± 0.96 ka.

The sediment chronologies for Doggerland extend back to approximately 14,000 to 15,000 years (Figure 12.9b), providing the temporal framework to interpret the late post-glacial landscape. From the onset of the freshwater sequence in core ELF034 to 12.67 ± 0.93 ka, to constraining the open estuary environment in core ELF045 to at least 13.39 ± 0.85 ka (bottom of unit not encountered), and shoreline deposits at the base of

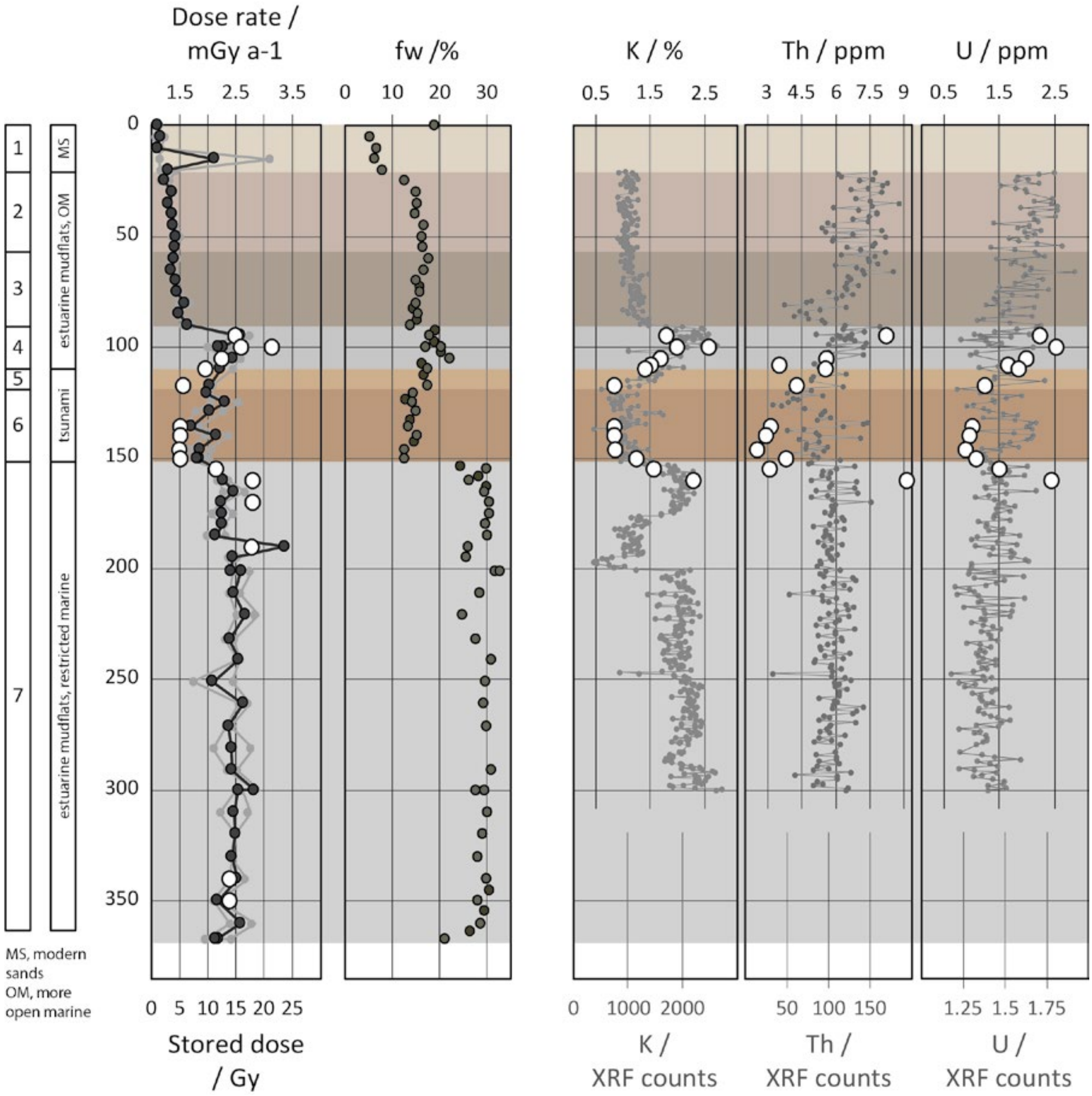


Figure 12.8 Dosimetry of core ELF001A: semi-quantitative and absolute down-core variations in radionuclide concentrations.

| Unit no. | Description / context | from samples | Age / ka |
|---|---|---|---|
| 1A-4 | laminated fine sands and silts; estuarine mudflats – open marine | 114/21, 114/22 | 6.03 ±0.22 |
| | | 114/23 | 7.16 ±0.50 |
| 1A-5 | grey silty fine sands, with shells; tsunami deposit | 114/24, 114/25 | 8.22 ±0.43 |
| 1A-6 | grey medium sands, v common shell fragments, small stones; tsunami deposit | 114/29, 114/30, 114/31, 114/32 | 8.04 ±0.43 |
| 1A-5 and 6 | | 114/24, 114/25,<br>114/29, 114/30, 114/31, 114/32 | 8.14 ±0.29 |

Table 12.2 Weighted combinations of OSL depositional ages for ELF001A.

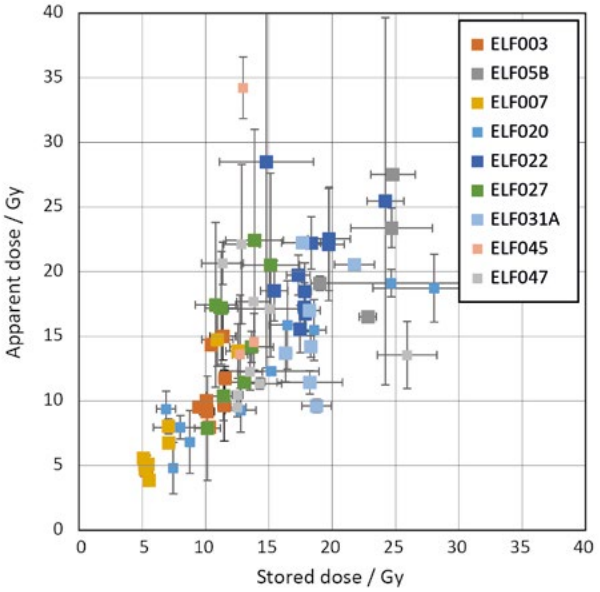


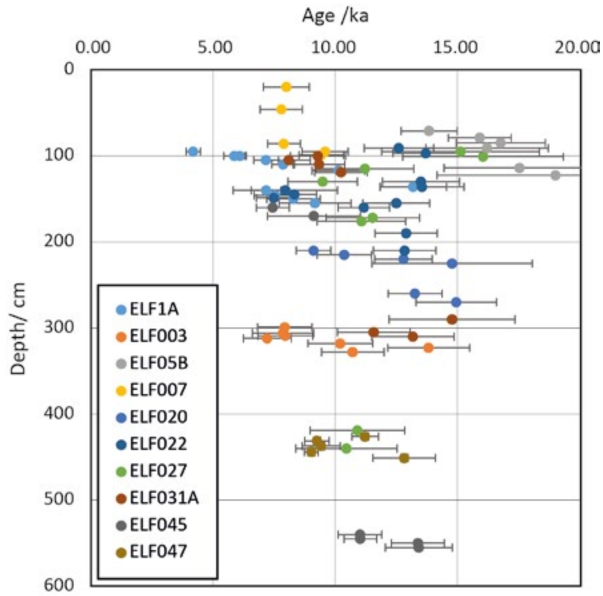


Figure 12.9 (left) Apparent vs stored dose estimates for discrete depths in core across a subset of sampled cores, encompassing terrestrial, littoral and marine deposits; (right) Quartz SAR OSL depositional ages shown relative to depth in core for the same subset of cores.

ELF003 to between 13.82 ± 1.68 ka to 10.20 ± 1.33 ka, with the weighted combination at 11.21 ± 1.04 ka.

OSL is also contributing to reconstructions for the period 14-7 ka, which is the period the sea is encroaching Doggerland, and palaeo-environments and geographies are rapidly evolving. Dating the development of strandlines at the Silver Pit, as preserved in core ELF027 between approximately 0.6 and 6.4m depth to 10.63 ± 0.74 ka. Providing temporal constraints for transgressions and regressions, such as 'dating' the transition from a littoral to more open marine, tidal mudflat setting at 4.3-4.4m depth in core ELF047 to after 9.11 +- 0.23 ka, or 'bracketing' the open estuarine environment in ELF045 to between 13.39 ± 0.85 ka to at least 10.97 ± 0.53 ka. OSL is also providing constraints on the terrestrial environments identified in core i.e. core ELF020, records the development of a wetland on a late-glacial landscape. The base of the wetland sequence is dated to 13.02 ± 1.26 ka, near contemporaneous, with disturbance to the underlying till, 37cm beneath palaeo-surface on which wetlands developed at 13.26 ± 1.10 ka.

## Conclusions

Luminescence investigations of the *Europe's Lost Frontiers* sedimentary cores from Dogger Bank are contributing to a high-resolution chronological framework for the terrestrial, near-shore and off-shore environments of Doggerland.